energy&fuels

pubs.acs.org/EF Article

Accelerating Fluid Development on a Chip for Renewable Energy

Junjie Zhong, Vikram Soni, Sepehr Saber, Jason Riordon, Bailey Schwarz, Matthew Toews, and David Sinton*

Cite This: https://dx.doi.org/10.1021/acs.energyfuels.0c01776 Read Online

ACCESS | Metrics & More | Article Recommendations

ABSTRACT: From physical property measurement to modelling pore-scale environments, the study of fluids at the microscale is key to understanding and optimizing fluids for large-scale energy applications. Silicon-glass microfluidics is now a proven technology for chemical effectiveness testing in the conventional oil and gas energy sector. We see potential to apply microfluidic fluid characterization technology to renewable sectors, such as geothermal and solar thermal energy recovery where fluid customization is central to performance. Key to unlocking performance gains in these renewable energy systems are phase change material slurries (PCSs)—fluids that exhibit a high apparent specific heat capacity. However, testing PCS synthesis recipes is currently a slow and expensive process, given the challenges of dynamic testing at process-relevant temperatures and pressures. In this work, we develop and test a robust silicon microfluidic device and measure important PCS emulsion properties including (i) viscosity, (ii) shear stability, (iii) phase change temperature/hysteresis, and (iv) phase change stability under dynamic conditions where tests are performed quickly (<1 h) and require only minimal test fluid volumes.

INTRODUCTION

The smallest fluid technologies have much to offer the world's large-scale fluid challenge—energy and associated CO_2. Over the last 10 years microfluidic methods have matured in two key application areas of particular value to the energy sector: the measurement of physical properties[1,2] and the physical modelling of the pore-scale environment.[3−5] In the area of fluid property measurement, microfluidics has proven useful in determining mutual (e.g., CO_2-oil) properties, such as diffusivities and solubilities,[6] as well as testing emulsion system behaviors.[7−9] Although microfabricated physical models of the porous media (or micromodels) long predate microfluidics,[10−12] modern fabrication (e.g., silicon-glass microfluidics) and microscopy methods have greatly expanded these capabilities leading to a wide range of applied pressures (up to 50 MPa)[13] and temperatures (up to 300 °C)[14] and the study of pore sizes at unprecedented small scales (down to sub-10 nm).[15−18]

The urgency to reduce CO_2 emissions and mitigate climate change is top-of-mind worldwide.[19−21] In addition to finding efficiencies in legacy energy systems, there is a growing need for new renewable energy capacity, as well as an emerging question: How can microfluidics be applied to advance renewable energy?[22,23] For example, enhanced geothermal energy recovery is a new application area, well suited to benefit from microfluidic tools. Specifically, the latest geothermal methods confine a working fluid in a closed loop to reduce the operational risk and lever powerful thermosiphon pumping.[24] The key to realizing the potential of this technology is finding a working fluid that is stable and maximizes energy recovery under harsh operating conditions. The size of the prize is immense: 1% of the thermal energy available from favorable geothermal locations worldwide matches the total current energy consumption globally.[25] Even a small increase in energy recovery would provide a large increase in the geothermal value proposition. Water is the most convenient working fluid currently used for geothermal recovery. Working fluids with emulsified phase change material—or phase change slurries (PCSs)—have potential to increase heat recovery but are largely untested.

PCS consists of a dispersed phase change material (PCM), such as paraffin, in a continuous fluid phase (e.g., water). It exhibits a high apparent specific heat capacity due to the large amounts of thermal energy stored or released in the form of latent heat as the PCM transforms from one phase to another.[26] Earlier research has focused on PCS potential in improving the efficiency of heat exchangers[27] and air conditioning.[28] It is increasingly apparent that PCS may well have a key role to play in enhancing renewable energy recovery (e.g., solar thermal[29] and geothermal[30]). In energy applications in general, there are many fundamental design challenges that need to be addressed experimentally, especially on PCS stability when PCS is used in a continuously flowing (and thus shearing) environment where phase change cycling is the norm.[31,32] Unstable fluid interfacial behaviors such as creaming, flocculation, and Ostwald ripening can lead to phase separation and eventually break the PCS emulsion system[32]—a costly outcome for renewable energy operators.

Received: June 2, 2020
Revised: July 25, 2020
Published: August 12, 2020

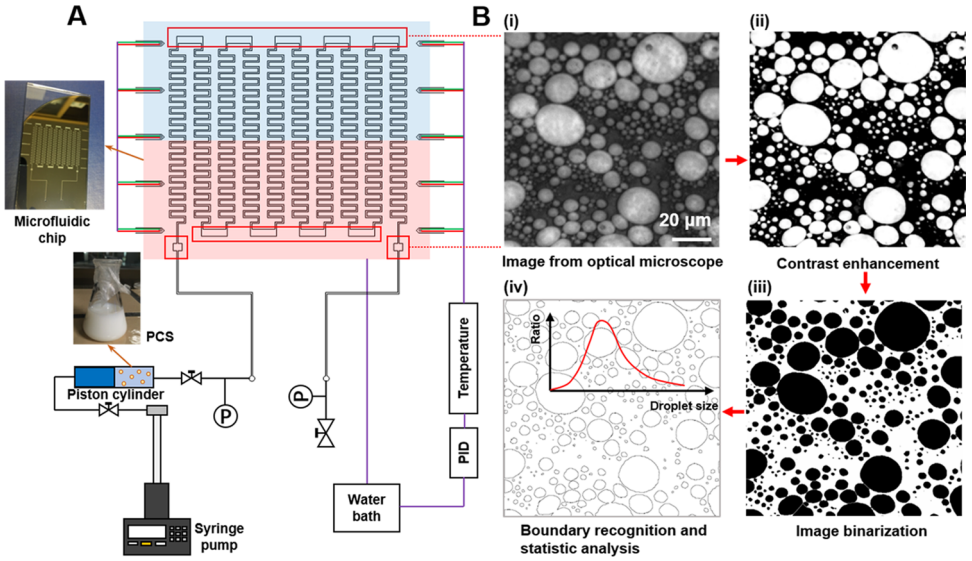

Figure 1. Schematic of the experimental system and emulsion analysis from a captured image. (A) Microfluidic chip with the pressure and temperature control system. (B) Emulsion in situ behavior observed under an optical microscope and with subsequent image processing as labeled.

Developing a PCS synthesis recipe for heat and energy application is simultaneously constrained by multiple variables (e.g., effective viscosity, emulsion stability, and phase change temperature hysteresis). PCS synthesis recipes have been developed to include different encapsulation strategies[33,34] and nanoparticles[35,36] for stabilizing the PCS to achieve the optimum heat management efficiency. The study of PCS conventionally requires multiple characterizing instruments and performing experiments that can be both time consuming (days to weeks per test)[32] and costly (e.g., differential scanning calorimetry at 10^3–10^4 k USD can provide thermal properties but not emulsion properties in flow conditions).[37,38] In this work, we demonstrate the application of a robust silicon microfluidic device for quantifying important PCS emulsion properties including (i) viscosity, (ii) shear stability, (iii) phase change temperature/hysteresis, and (iv) phase change stability. The key innovation here is that PCS property tests are performed within a single device, using only micro- to milliliters of the PCS fluid sample, and requiring less than 1 h. Direct observation through the microfluidic chip allows in situ statistical emulsion analysis for future PCS recipe design and optimization. This PCS serves as one example of industrial fluid development for renewable energy recovery. We anticipate a bright future for microfluidic-based analyses of industrial fluids more generally, with potential to realize fully automated industrial fluid development (synthesis, testing, and optimization), following the emerging model for chemical synthesis.[39]

MATERIALS AND METHODS

Phase Change Slurry Synthesis. We synthesized a working PCS with 40% (weight ratio) *n*-hexadecane (Sigma-Aldrich). The surfactant for generating a stable oil–water (o/w) emulsion is a mixture of Span 80 and Tween 80 (weight ratio = 2:3) with a hydrophilic–lipophilic balance (HLB) value of 10.7. The total weight ratio for the surfactant was 5% (thus hexadecane/surfactant/water = 0.4:0.05:0.55). The surfactant was first mixed with hexadecane at 80 °C with continuous stirring at 600 rpm for 1 min. Then, water was added at 2 mL/min at the same temperature and stirring rate. Next, the emulsion was stirred at 600 rpm for 10 more minutes to achieve better mixing quality and then fast cooled (5 min) to 20 °C in a water bath. The heating, stirring, and fast cooling procedure was repeated three times to increase the emulsion interfacial stability.[40] The synthesized PCS was then transferred to a high-pressure piston cylinder (HIP 70C3-10-P). The working PCS synthesized here is not necessarily suitable for a practical heat recovery system. However, the current study delineates the methodology of using microfluidics to characterize PCS properties, and the relevant fundamental PCS mechanisms. In engineering applications, the paraffin should be selected based on the heat reservoir temperature conditions. Commercial paraffin blends usually cover a wide working temperature range for different applications.

Microfluidic Chip Fabrication and Experimental System Design. The microfluidic chip was designed with a long (1 m) microchannel (200 μm × 20 μm) to provide significant shear exposure of the fluid, for studying the shear effect on emulsion properties (Figure 1A). A silicon wafer was used to fabricate the chip with standard dry etching (DRIE), which guaranteed a channel surface roughness below 1 μm. Anodic bonding was performed with borosilicate glass to provide in situ and real-time observation of the emulsion through an optical microscope (Figure 1B) and allow for a high pressure and temperature tolerance (10 MPa and 200 °C). Eleven observation windows (1 mm wide and 20 μm deep) were distributed evenly along the channel (Figure 1A) for different measurement requirements. The images/videos were taken during experiments and were then analyzed with ImageJ via the procedure shown in Figure 1B.

To control and monitor the testing pressure, the microfluidic chip was connected to a fluid regulating system (a piston cylinder containing PCS, an ISCO syringe pump, and pressure transducers), with a manifold fabricated in-house. For temperature control, the silicon side of the chip was attached to two copper blocks controlled by two water baths (Cole-Parmer Polystat standard 6.5 L bath), which could generate either a uniform temperature or a temperature gradient on the device. Ten thermocouples were inserted into the chip through deep thermocouple channels (700 μm × 400 μm) etched close to the microchannel to map the temperature field (Figure 1A) and provide feedback to control two water baths.

The microfluidic chip and the P-T control units together established an on-chip heat exchanger that can monitor in situ PCS behaviors under different dynamic conditions. Renewable thermal energy recovery systems, such as geothermal and solar thermal, are essentially combinations of heat exchangers at large scales, where some important working fluid features can be efficiently analyzed through the on-chip heat exchanger.

https://dx.doi.org/10.1021/acs.energyfuels.0c01776
Energy Fuels XXXX, XXX, XXX–XXX

RESULTS AND DISCUSSION

PCS Emulsion Viscosity vs Shear Rate. An emulsion fluid system can exhibit non-Newtonian fluid behavior, where the viscosity of the emulsion varies with shear rate.[41] A rheometer is generally used to study this behavior.[31] Here, we demonstrated that the microfluidic device can serve the same purpose faster by directly quantifying the relation between the fluid viscosity and shear rate by measuring the emulsion flow velocity under a given pressure drop in the microchannel. When a laminar flow is established in a microchannel, the fluid viscosity (η) and maximum shear rate at the microchannel wall ($\dot{\gamma}$) can be expressed as measurables or known parameters

$$\eta = \frac{h^2 \Delta P}{12 L v} \tag{1}$$

$$\dot{\gamma} = \frac{6v}{h} \tag{2}$$

where h is the microchannel height and L is the total length of the microchannel—both are known parameters from the microfluidic chip design and fabrication. ΔP is the total pressure drop along the flow direction and is controlled via the pump and measured by two pressure transducers at the inlet and outlet of the chip (Figure 1A). v is the average flow velocity of the emulsion over the microchannel cross section, which is directly measured from the microscope images/videos. For the working PCS emulsion, we controlled the flow in the chip and maintained a constant temperature (20 °C) and different pressure drops (0.1−0.5 MPa in 0.1 MPa steps, 0.5−2.5 MPa in 0.5 MPa steps). To measure the average emulsion flow velocity, we randomly selected a droplet in the flow, and tracked the droplet position as a function of time to calculate the droplet velocity (Figure 2A). By selecting three different locations from the upstream to the downstream of the microchannel (Figure 2B), the average emulsion flow velocity in the microchannel is assumed to be the average of the droplet velocities. From eqs 1 and 2, the PCS viscosities at different shear rates were calculated and plotted, as shown in Figure 2B, where a typical shear-thinning behavior (i.e., decreasing viscosity with increasing shear rate) for the working PCS was observed. The experimental data was fit to the Carreau equation for describing the shear-thinning behavior[42]

$$\eta = \eta_\infty + (\eta_o - \eta_\infty)\left[1 + \left(\frac{\dot{\gamma}}{\dot{\gamma}_m}\right)^2\right]^{n-1/2} \tag{3}$$

where η_o is the PCS viscosity at the zero shear rate, η_∞ is the PCS viscosity at the infinite shear rate (usually fixed as 0), $\dot{\gamma}_m$ is the transition shear rate where the fluid viscosity transforms from Newtonian to non-Newtonian behaviors, and n is a dimensionless power-law fluid flow behavior index. The theoretical description of the PCS non-Newtonian behavior can be obtained by fitting η_o, $\dot{\gamma}_m$, and n in eq 3 with experimental data. For the working PCS, the η_o, $\dot{\gamma}_m$, and n are fitted to be 0.11 Pa·s, 33 s^{-1}, and 0.65. The prediction from the Carreau equation of the working PCS is also shown in Figure 2B. In addition to providing important fundamental understanding of the PCS non-Newtonian behavior with η_o and $\dot{\gamma}_m$, the equation is readily applicable to any simulations using the same PCS.[43]

The viscosity of the PCS emulsion is in general much higher than water (e.g., here up to 10^2 times higher), which leads to practical concerns of pumping costs. At the same flow rate, the higher viscosity leads to a lower Reynolds number and thus a larger frictional coefficient from the Moody diagram. The increased frictional loss must be compensated by additional pumping power. Reducing the emulsion viscosity lessens the pressure loss along the flow direction, and is beneficial for energy applications to further improve the system efficiency.[44] There are many viscosity-reducing agents that have been proven to work well for emulsions in the oil and gas industry through bulk experiments (e.g., core flooding), targeting specifically enhanced heavy oil production.[45] The microfluidic device developed here allows quick (<1 h) and direct measurements of the viscosities of emulsions synthesized by different recipes and under a range of shear rate conditions meeting practical application requirements. The device is thus a useful platform to quickly assess and screen viscosity-reducing agents for PCS, and more generally for applications of emulsions where the non-Newtonian fluid behavior is of importance.[46] In addition, many other factors that will potentially affect the emulsion viscosity, such as the fluid temperature,[47] mass ratio of different components,[32] and emulsion droplet size,[48] can also be evaluated.

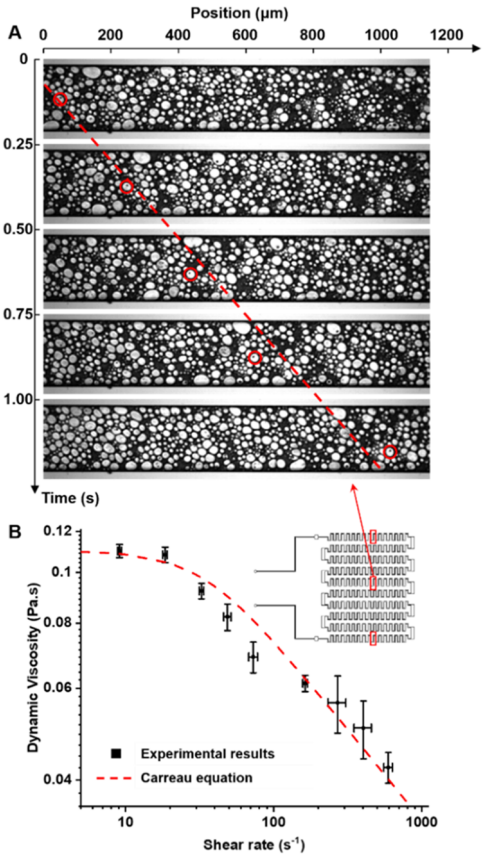

Figure 2. PCS emulsion viscosity vs shear rate. (A) Measuring emulsion velocity by tracking oil droplets traveling in a microchannel. Here the pressure difference between the inlet and the outlet of the microchannel is 1.5 MPa (shear rate of 270 s^{-1}). (B) PCS viscosity measured at different shear rates, with the Carreau equation predicting the shear-thinning behavior. The testing uncertainty of the measured dynamic viscosity is defined by the maximum testing error to be 6.7%.

PCS Shear Stability. Using PCS for heat and energy recovery requires continuous mechanical loading and cycling of PCS in a flow loop for a long period (months to years).[32]

https://dx.doi.org/10.1021/acs.energyfuels.0c01776
Energy Fuels XXXX, XXX, XXX−XXX

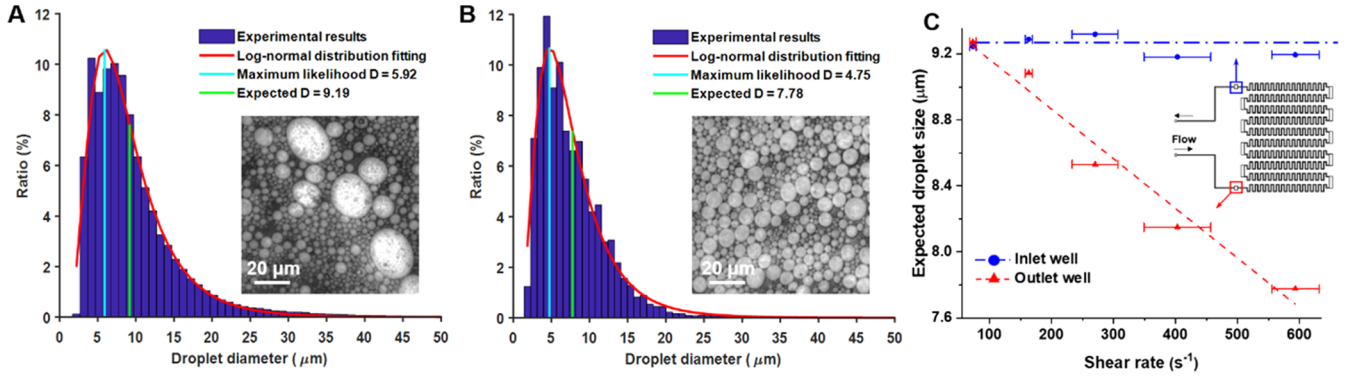

Figure 3. PCS emulsion droplet size change vs shear rate. (A) Emulsion droplet size distribution at the microfluidic chip inlet well. (B) Emulsion droplet size distribution at the microfluidic chip outlet well. Here, the applied pressure difference between the inlet and outlet of the microchannel is 2.5 MPa (shear rate = 590 s^{-1}). (C) Expected (average) droplet size change as a function of shear rate, where the shear stress contributes to reduce the overall emulsion droplet size and thus stabilizes the PCS. The testing uncertainty for the droplet size is defined by the error of shear rates to be 17.5%.

PCS emulsion fluid mechanical stability (even while under high shear stress) is key to maintaining high heat management performance and efficiency in the system. The PCS shear stability is conventionally tested by circulating the PCS in bulk piping and then comparing the emulsion droplet size distribution variation before and after the circulation with a laser scattering droplet size analyzer.[32]

The microfluidic device allows direct quantification of the role of shear stress on emulsion stability in parallel to viscosity measurements by comparing the emulsion droplet size distribution change between the inlet and outlet of the microchannel (Figure 3). For example, when setting the pressure drop along the microchannel to 2.5 MPa, the shear rate of the emulsion is calculated from eq 2 to be 590 s^{-1}. After the flow is well established in the microchannel, we recorded a video continuously for 3 min at both the inlet and the outlet well of the microfluidic chip (Figure 3). Statistical analysis (Figure 1B) of each frame from the video (~10 fps) produced the droplet size distributions shown in Figure 3A,B, where both the maximum likelihood droplet size and the expected droplet size were calculated. The emulsion droplet sizes of each observed population were reduced from the inlet to the outlet; the maximum likelihood droplet size reduced by 19.7% and the expected droplet size reduced by 15.4%. This reduction was attributed to the strong shear force during the flow. We assessed the shear effect at different shear rate values, and a linear trend was found (Figure 3C).

The testing shear rates here are in the typical range of many heat energy systems such as surface heat exchangers ($10-10^3$ s^{-1}).[49] The smaller emulsion droplet diameter at the chip outlet compared to the diameter at the inlet indicates that the shear force helps to maintain the emulsion fluid mechanical stability. According to Stoke's law, a smaller emulsion droplet size has a lower rising velocity ($u \propto D^2$), which leads to a lower chance for emulsion droplets to coalesce and cream.[50]

Once the channel/pipe size and flow rate change, the maximum shear rate will change accordingly. The microfluidic device provides the chance to measure viscosity in a wide range of shear rates by alternating the pressure drop, covering different PCS working conditions. Although the emulsion flow in the microfluidic device is laminar, with a low Reynold number (here on the order of $10^{-3}-10^{-2}$ due to the microchannel size 10^{-5} m), the shear rates achieved here match well with those of large-scale, turbulent flow applications of interest. In a bulk flow with the same emulsion, these shear rates are reached only in the laminar viscous shear layer at the wall in an otherwise turbulent flow (e.g., a pipe diameter at 10^{-1} m with $Re = 10^5-10^6$). The experimental results of fluid behaviors from laminar flow tests can thus recreate the maximum shear rate conditions expected in large-scale applications.[51] In addition, the microfluidic device could also provide data to capture the local flow behaviors around a PCM droplet (i.e., Stokes flow) for bulk scale applications. A full scan of the magnitudes of bulk shear rate conditions in the microfluidic chip provides a complete characterization of emulsion fluid mechanical stability expected in the larger systems of interest.

PCS Emulsion Droplet Solidifying Ratio vs Subcooling. Applying PCS for heat management involves many cycles of PCM solidification and melting, and the solidifying/melting temperatures are key parameters to be characterized. The solidifying temperature of liquid droplets can be notably reduced from the bulk freezing point when the droplet radius is at the micrometer scale and below—an effect known as capillary solidifying point depression—and described through the Gibbs–Thomson equation[52]

$$\Delta T_s = T_s^{bulk} - T_s^{droplet} = \frac{4\sigma_{sl} T_s^{bulk}}{dL\rho_{solid}} \quad (4)$$

where ΔT_s is the solidifying temperature reduction from the bulk, T_s^{bulk} is the liquid bulk solidifying temperature (for hexadecane the temperature is 18 °C), $T_s^{droplet}$ is the solidifying temperature of the liquid droplet, σ_{sl} is the interfacial tension between the liquid and solid phases (up to 100 mN/m), d is the droplet diameter (here ~10 μm), L is the latent heat of freezing (for hexadecane it is 227 kJ/kg),[53] and ρ_{solid} is the solid density (~770 kg/m^3). From eq 4, a theoretical prediction for the maximum solidifying temperature reduction of the working PCS here is 0.07 °C. However, a previous experimental study indicates a much larger solidifying temperature reduction, by up to two orders of magnitude greater than the theoretical prediction (i.e., ~10 °C).[54] Such a huge deviation of solidifying temperature between the theoretical prediction and experimental results is potentially attributed to the kinetic effect of crystallization,[55] as the crystallization rate is directly associated with the emulsion droplet size. According to the classical nucleation theory,[56] the

https://dx.doi.org/10.1021/acs.energyfuels.0c01776
Energy Fuels XXXX, XXX, XXX−XXX

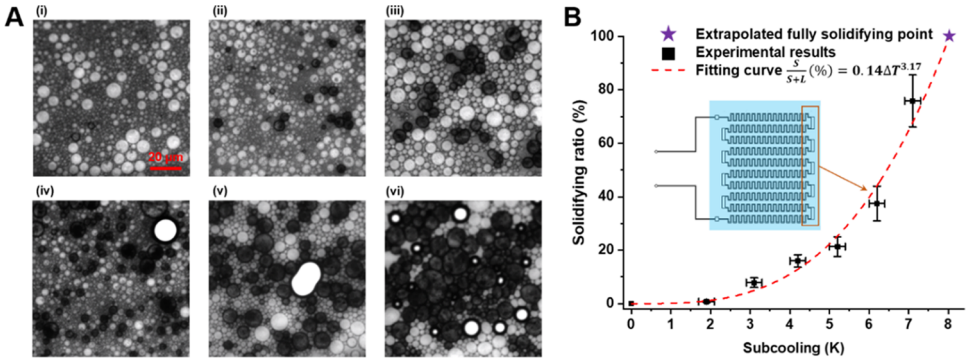

Figure 4. PCS emulsion droplet solidifying ratio vs subcooling. (A) Direct observation of PCS solidifying result at subcooling is (i) 1.9 K, (ii) 3.1 K, (iii) 4.2 K, (iv) 5.2 K, (v) 6.2 K, and (vi) 7 K. The dark circles are the solid hexadecane particles, the gray circles are the liquid hexadecane droplets, and the bright circles are air initially dissolved in the PCS mixture. (B) Experimental results of hexadecane solidifying ratio vs subcooling. The error bar represents the variation across five different observation windows (error for the *y* axis) and temperature uncertainty across the chip (error for the *x* axis). The extrapolated fully solidifying point is obtained by fitting the empirical formula of the solidifying PCM particle ratio (ø)—solid particles (S)/(solid particles (S) + liquid droplets (L))—vs subcooling, using experimental results. The testing uncertainty of the measured solidifying ratio is defined by the maximum testing error to be 7.9%.

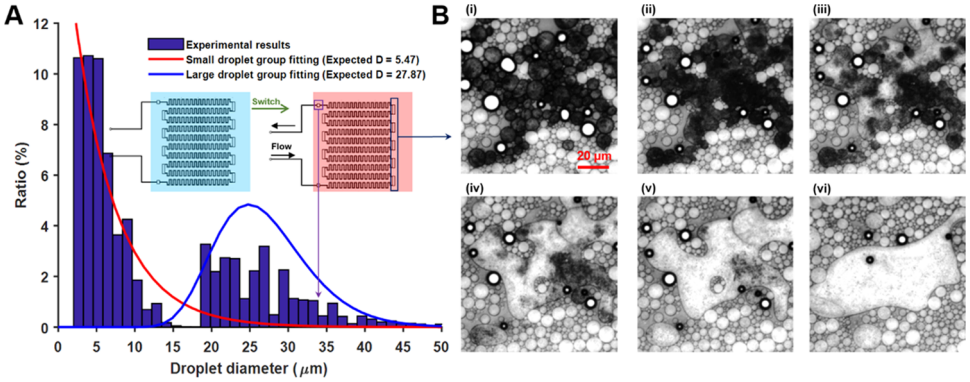

Figure 5. PCS microdroplet merging after melting. (A) Emulsion droplet size distribution at the microfluidic chip outlet well after a solidifying–melting cycle. The applied pressure drop is 2.5 MPa and a peak on large droplets (20–40 μm) is observed in addition to small droplets (<15 μm) due to shear. (B) Direct observation of multiple solid hexadecane microparticles melting and merging into a large hexadecane droplet (i–vi). The air bubble dissolved into the PCS mixture during melting.

solidifying PCM particle ratio (ø) changing with time (t) can be expressed as

$$\text{ø} = 1 - \exp(-kt) \tag{5}$$

where k is the homogeneous nucleation rate for crystallization

$$k = AV_{\text{d}} \exp\left(\frac{-\Delta G^*}{k_{\text{B}}T}\right) \tag{6}$$

where A is a rate constant, V_{d} is a single PCM droplet size, k_{B} is the Boltzmann constant, T is the emulsion temperature, and ΔG^* represents the energy barrier for the PCM liquid droplet transiting to the solid particle

$$\Delta G^* = \frac{16}{3}\frac{\sigma^3 v^2}{L^2}\left(\frac{T_{\text{s}}^{\text{droplet}}}{T_{\text{s}}^{\text{droplet}} - T}\right) \tag{7}$$

where σ is the PCM solid–liquid interfacial tension, v is the nucleus size, and L is the latent heat of fusion. From eq 5, given a certain amount of experimental duration, the nucleation rate determines the total solid particles that can be detected. From eqs 6 and 7, one finds for a small droplet size, k is low, which potentially leads to undetectable solidification within the experimental duration. To achieve faster solidification to be detected within the same duration, reducing the emulsion temperature is practical and results in a low solidification temperature to be detected. Therefore, a case-by-case test for the PCS solidifying temperature is essential for various applications, in terms of a specific droplet size and a required duration for the phase change.

Measuring the PCS solidifying point is conventionally performed by differential scanning calorimetry (DSC).[32] Here, we demonstrate that microfluidic devices can conveniently measure the PCS solidifying temperature and solidifying temperature hysteresis by directly observing the emulsion phase transition under different temperature conditions.

To perform the PCS solidifying test, we injected the PCS with the PCM at the liquid phase into the microchannel and controlled the chip temperature at different testing solidifying temperatures. The tested subcooling (i.e., bulk solidifying temperature–experimental temperature) ranged from 2 to 7 °C (1 °C as the temperature step), and in each temperature condition, we waited for 30 min to ensure that the near-equilibrium condition of the phase change had been achieved (e.g., solid phase barely changing within 5 min). Figure 4A shows a microscope image of the emulsion solidifying results at different subcooling conditions. Based on the image, the solidifying ratio is defined as the ratio between solid hexadecane particles (dark) and the sum of hexadecane

https://dx.doi.org/10.1021/acs.energyfuels.0c01776
Energy Fuels XXXX, XXX, XXX–XXX

droplets (gray) and solid hexadecane particles. As shown in Figure 4B, the solidifying ratio is found to increase with subcooling and reaches 76 ± 10% at 7 °C. By further fitting the experimental data with a polynomial function, an empirical formula for PCS solidifying ratio vs subcooling was obtained (Figure 4B). From the empirical formula, the extrapolated fully solidifying (i.e., 100% solidifying ratio) subcooling is 7.9 °C, which closely matches previous experimental results from DSC tests of paraffin-based PCS.[32]

In practice, a large subcooling of PCM is not favorable as it can significantly reduce the system energy efficiency.[57] In addition to the emulsion droplet size and the presence of the surfactant, there are many other factors that can affect PCS subcooling, such as the emulsion shear rate.[54] These factors are readily quantified with the microfluidic device. To suppress the large subcooling required, nucleating agents, such as nanoparticles,[58] can be added into the PCS emulsion to promote heterogeneous nucleation. Importantly, the microfluidic chip can serve as a platform to innovate and screen different nucleating agent recipes and strategies for efficient PCS applications.

Droplet Coalescence during PCS Emulsion Melting. The PCS stability during phase change cycling (melting and solidification) is another important consideration, in addition to the fluid mechanical stability discussed earlier. A previous study has shown that after loading the paraffin-based PCS in heating−cooling cycles for three days, the distribution of the emulsion droplet size shifts from a unimodal distribution (peak at ∼3 μm) to a bimodal distribution with a second droplet size peak appearing at ∼30 μm.[32] An emulsion droplet that becomes larger during phase change cycling indicates potential for unstable emulsion phase separation—a risk to operations.

We performed microfluidic tests to directly study the fundamental mechanism behind this phenomenon. As shown in Figure 5A, the microfluidic chip filled with PCS was first cooled to 11 °C (7 °C subcooling) for 30 min to allow most hexadecane liquid microdroplets to transform to the solid phase and reach near-equilibrium. Next, we heated the chip to 25 °C, where solid hexadecane is expected to melt. A pressure of 2.5 MPa was then applied to drive the melted PCS under shear in the microchannel. We quantified the emulsion droplet size distribution at the outlet well (Figure 5A). Similar to previous bulk tests,[32] a bimodal distribution of droplet sizes was observed, with a new peak appearing at ∼25 μm compared to the case without the phase change (Figure 3B, the droplet size distribution is unimodal and the peak is at 4.8 μm).

The fundamental mechanism of PCS emulsion droplet size growth after phase change cycling is due to the merging of small solid PCM particles during melting. The nonionic surfactant molecules (here Span 80 and Tween 80) initially kept the size of oil droplets small but fail to sufficiently cover the droplet surfaces after melting. The microfluidic chip allows direct observation of this process, as shown in Figure 5B. An emulsion droplet that becomes larger during phase change cycling indicates the potential for unstable emulsion phase separation under shearing. Once the PCS flow system is scaled, there is concern that large PCM droplets solidify and cease to be carried as efficiently by the continuous flow. The large solid PCM particles could accumulate and block the pipe, posing a risk to renewable energy recovery operations. However, when PCS is in a continuous flow condition (e.g., heat exchanger), the shear stress is expected to reduce the large droplet size as discussed previously (Figure 3), especially in a turbulent flow environment. In case the shear stress is not sufficiently high to ensure emulsion stability during the phase change cycle, it is necessary to either change the surfactant species to increase the repulsive force between PCM droplets (e.g., adding ionic surfactant species with the electrostatic force)[59] or encapsulate the emulsion droplet with polymers or nanoparticles so that the PCM droplets are isolated from each other.[60] The microfluidic strategy developed here allows immediate screening of the surfactant recipes and the study of the effect of encapsulation by directly capturing the potential droplet merging risk (Figure 5B). The device allows for much faster analysis (<1 h) compared to classical tests in bulk fluids that require several days to weeks for cycling PCS and measuring the droplet size distribution change.[32]

CONCLUSIONS

In this work, we demonstrated a silicon microfluidic device for characterizing PCS properties at dynamic conditions including emulsion viscosity change with shear stress, shear stability defined by the emulsion droplet size change, solidifying temperature/subcooling as well as melting instability and mechanism. Conventional methods, such as laser scattering particle size distribution analysis and differential scanning calorimetry, tend to provide fluid properties at stagnant conditions. While static fluid properties are vital, working fluids in renewable thermal energy recovery systems mostly experience dynamic conditions, and microfluidic devices can exactly establish the bridge between the lab test results and real applications. Also compared to conventional methods, the microfluidic device provides higher throughput (on the order of 10 min/test and <1 h for all), lower cost (<1 k USD/chip and reusable), and less fluid sample required (microlitre to milliliter). The detection procedures take full advantage of silicon-glass microfluidics in terms of direct and real-time visualization, accurate temperature control/measurement, and high-pressure/chemical tolerance. The result is a rich PCS fluid data set. More broadly, our approach demonstrates that silicon-glass microfluidics has a bright future in industrial fluid synthesis and testing for the renewable sector.

Looking forward, we see great potential in adding fluid thermal sensors within the silicon microfluidic device, i.e., an on-chip calorimeter, where the fluid thermal conductivity, thermal capacity, and phase change latent heat can be accurately measured. A future silicon microfluidic device could combine the flow testing abilities demonstrated here and powerful thermal measurements, which would also provide heat transfer quantification on a chip. For the PCS, the heat transfer coefficients at different flow rates and phase conditions are directly related to the overall heat recovery performance. We envision a microfluidic toolbox to efficiently and cheaply quantify a set of on-demand industrial fluid properties (both fluid mechanical properties and thermal properties) that are difficult or impossible to obtain by conventional instruments.

AUTHOR INFORMATION

Corresponding Author

David Sinton − *Department of Mechanical and Industrial Engineering, University of Toronto, Ontario, Toronto M5S 3G8, Canada;* orcid.org/0000-0003-2714-6408; Email: sinton@mie.utoronto.ca

https://dx.doi.org/10.1021/acs.energyfuels.0c01776
Energy Fuels XXXX, XXX, XXX−XXX

Authors

Junjie Zhong − *Department of Mechanical and Industrial Engineering, University of Toronto, Ontario, Toronto M5S 3G8, Canada;* orcid.org/0000-0001-6293-9580

Vikram Soni − *Department of Mechanical and Industrial Engineering, University of Toronto, Ontario, Toronto M5S 3G8, Canada*

Sepehr Saber − *Department of Mechanical and Industrial Engineering, University of Toronto, Ontario, Toronto M5S 3G8, Canada*

Jason Riordon − *Department of Mechanical and Industrial Engineering, University of Toronto, Ontario, Toronto M5S 3G8, Canada*

Bailey Schwarz − *Eavor Technologies Inc., Calgary, Alberta T2P 3H9, Canada*

Matthew Toews − *Eavor Technologies Inc., Calgary, Alberta T2P 3H9, Canada*

Complete contact information is available at: https://pubs.acs.org/10.1021/acs.energyfuels.0c01776

Notes

The authors declare no competing financial interest.

■ ACKNOWLEDGMENTS

The authors gratefully acknowledge support from Eavor Technologies as well as the Natural Sciences and Engineering Council of Canada (NSERC) for their funding support through partnership programs, the Discovery Grant Program, the Discovery Accelerator Program, and an E.W.R. Steacie Memorial Fellowship (D.S.). Support through the Canada Foundation for Innovation and the Ontario Research Fund is also gratefully acknowledged.

■ REFERENCES

(1) Song, W.; Fadaei, H.; Sinton, D. Determination of Dew Point Conditions for CO_2 with Impurities Using Microfluidics. *Environ. Sci. Technol.* **2014**, *48*, 3567−3574.

(2) Mostowfi, F.; Molla, S.; Tabeling, P. Determining phase diagrams of gas−liquid systems using a microfluidic PVT. *Lab Chip* **2012**, *12*, 4381−4387.

(3) Anbari, A.; Chien, H. T.; Datta, S. S.; Deng, W.; Weitz, D. A.; Fan, J. Microfluidic model porous media: fabrication and applications. *Small* **2018**, *14*, No. 1703575.

(4) Yoon, H.; Chojnicki, K. N.; Martinez, M. J. Pore-Scale Analysis of Calcium Carbonate Precipitation and Dissolution Kinetics in a Microfluidic Device. *Environ. Sci. Technol.* **2019**, *53*, 14233−14242.

(5) He, D.; Jiang, P.; Xu, R. Pore-Scale Experimental Investigation of the Effect of Supercritical CO_2 Injection Rate and Surface Wettability on Salt Precipitation. *Environ. Sci. Technol.* **2019**, *53*, 14744−14751.

(6) Sharbatian, A.; Abedini, A.; Qi, Z.; Sinton, D. Full characterization of CO_2−oil properties on-chip: solubility, diffusivity, extraction pressure, miscibility, and contact angle. *Anal. Chem.* **2018**, *90*, 2461−2467.

(7) Nowbahar, A.; Whitaker, K. A.; Schmitt, A. K.; Kuo, T.-C. Mechanistic Study of Water Droplet Coalescence and Flocculation in Diluted Bitumen Emulsions with Additives Using Microfluidics. *Energy Fuels* **2017**, *31*, 10555−10565.

(8) Dudek, M.; Chicault, J.; Øye, G. Microfluidic Investigation of Crude Oil Droplet Coalescence: Effect of Oil/Water Composition and Droplet Aging. *Energy Fuels* **2020**, *34*, 5110−5120.

(9) Yu, F.; Jiang, H.; Fan, Z.; Xu, F.; Su, H.; Li, J. Formation and Flow Behaviors of in Situ Emulsions in Heavy Oil Reservoirs. *Energy Fuels* **2019**, *33*, 5961−5970.

(10) Lin, Y.-J.; Cao, T.; Chacón-Patiño, M. L.; Rowland, S. M.; Rodgers, R. P.; Yen, A.; Biswal, S. L. Microfluidic Study of the Deposition Dynamics of Asphaltene Subfractions Enriched with Island and Archipelago Motifs. *Energy Fuels* **2019**, *33*, 1882−1891.

(11) Lin, Y.-J.; He, P.; Tavakkoli, M.; Mathew, N. T.; Fatt, Y. Y.; Chai, J. C.; Goharzadeh, A.; Vargas, F. M.; Biswal, S. L. Characterizing Asphaltene Deposition in the Presence of Chemical Dispersants in Porous Media Micromodels. *Energy Fuels* **2017**, *31*, 11660−11668.

(12) Nooraiepour, M.; Fazeli, H.; Miri, R.; Hellevang, H. Effect of CO_2 Phase States and Flow Rate on Salt Precipitation in Shale Caprocks—A Microfluidic Study. *Environ. Sci. Technol.* **2018**, *52*, 6050−6060.

(13) Gothsch, T.; Schilcher, C.; Richter, C.; Beinert, S.; Dietzel, A.; Büttgenbach, S.; Kwade, A. High-pressure microfluidic systems (HPMS): flow and cavitation measurements in supported silicon microsystems. *Microfluid. Nanofluid.* **2015**, *18*, 121−130.

(14) Cheng, X.; Ooms, M. D.; Sinton, D. Biomass-to-biocrude on a chip via hydrothermal liquefaction of algae. *Lab Chip* **2016**, *16*, 256−260.

(15) Zhong, J.; Alibakhshi, M. A.; Xie, Q.; Riordon, J.; Xu, Y.; Duan, C.; Sinton, D. Exploring Anomalous Fluid Behavior at the Nanoscale: Direct Visualization and Quantification via Nanofluidic Devices. *Acc. Chem. Res.* **2020**, *53*, 347−357.

(16) Zhong, J.; Talebi, S.; Xu, Y.; Pang, Y.; Mostowfi, F.; Sinton, D. Fluorescence in sub-10 nm channels with an optical enhancement layer. *Lab Chip* **2018**, *18*, 568−573.

(17) Yang, Q.; Jin, B.; Banerjee, D.; Nasrabadi, H. Direct visualization and molecular simulation of dewpoint pressure of a confined fluid in sub-10 nm slit pores. *Fuel* **2019**, *235*, 1216−1223.

(18) Jatukaran, A.; Zhong, J.; Abedini, A.; Sherbatian, A.; Zhao, Y.; Jin, Z.; Mostowfi, F.; Sinton, D. Natural gas vaporization in a nanoscale throat connected model of shale: multi-scale, multi-component and multi-phase. *Lab Chip* **2019**, *19*, 272−280.

(19) Figueres, C.; Le Quéré, C.; Mahindra, A.; Bäte, O.; Whiteman, G.; Peters, G.; Guan, D. Emissions are still rising: ramp up the cuts. *Nature* **2018**, *564*, 27−30.

(20) Kharecha, P. A.; Kutscher, C. F.; Hansen, J. E.; Mazria, E. Options for Near-Term Phaseout of CO_2 Emissions from Coal Use in the United States. *Environ. Sci. Technol.* **2010**, *44*, 4050−4062.

(21) Kang, J.; Ng, T. S.; Su, B.; Yuan, R. Optimizing the Chinese Electricity Mix for CO_2 Emission Reduction: An Input−Output Linear Programming Model with Endogenous Capital. *Environ. Sci. Technol.* **2020**, *54*, 697−706.

(22) Matuszek, K.; Vijayaraghavan, R.; Forsyth, C. M.; Mahadevan, S.; Kar, M.; MacFarlane, D. R. Pyrazolium Phase-Change Materials for Solar-Thermal Energy Storage. *ChemSusChem* **2020**, *13*, 159−164.

(23) Sinton, D. Energy: the microfluidic frontier. *Lab Chip* **2014**, *14*, 3127−3134.

(24) Sun, F.; Yao, Y.; Li, G.; Li, X. Geothermal energy development by circulating CO2 in a U-shaped closed loop geothermal system. *Energy Convers. Manage.* **2018**, *174*, 971−982.

(25) Limberger, J.; Boxem, T.; Pluymaekers, M.; Bruhn, D.; Manzella, A.; Calcagno, P.; Beekman, F.; Cloetingh, S.; van Wees, J.-D. Geothermal energy in deep aquifers: A global assessment of the resource base for direct heat utilization. *Renewable Sustainable Energy Rev.* **2018**, *82*, 961−975.

(26) Ma, F.; Zhang, P. A review of thermo-fluidic performance and application of shellless phase change slurry: Part 1−Preparations, properties and applications. *Energy* **2019**, *189*, No. 116246.

(27) Delgado, M.; Lázaro, A.; Mazo, J.; Zalba, B. Review on phase change material emulsions and microencapsulated phase change material slurries: materials, heat transfer studies and applications. *Renewable Sustainable Energy Rev.* **2012**, *16*, 253−273.

(28) Diaconu, B. M.; Varga, S.; Oliveira, A. C. Experimental assessment of heat storage properties and heat transfer characteristics of a phase change material slurry for air conditioning applications. *Appl. Energy* **2010**, *87*, 620−628.

(29) Ma, F.; Zhang, P. Heat Transfer Characteristics of a Volumetric Absorption Solar Collector using Nano-Encapsulated Phase Change Slurry. *Heat Transfer Eng.* **2018**, *39*, 1487−1497.

(30) Nazir, H.; Batool, M.; Osorio, F. J. B.; Isaza-Ruiz, M.; Xu, X.; Vignarooban, K.; Phelan, P.; Kannan, A. M. Recent developments in phase change materials for energy storage applications: a review. *Int. J. Heat Mass Transfer* **2019**, *129*, 491−523.
(31) Huang, L.; Petermann, M. An experimental study on rheological behaviors of paraffin/water phase change emulsion. *Int. J. Heat Mass Transfer* **2015**, *83*, 479−486.
(32) Huang, L.; Petermann, M.; Doetsch, C. Evaluation of paraffin/water emulsion as a phase change slurry for cooling applications. *Energy* **2009**, *34*, 1145−1155.
(33) Magendran, S. S.; Khan, F. S. A.; Mubarak, N. M.; Vaka, M.; Walvekar, R.; Khalid, M.; Abdullah, E. C.; Nizamuddin, S.; Karri, R. R. Synthesis of organic phase change materials (PCM) for energy storage applications: A review. *Nano-Struct. Nano-Objects* **2019**, *20*, No. 100399.
(34) Huang, X.; Zhu, C.; Lin, Y.; Fang, G. Thermal properties and applications of microencapsulated PCM for thermal energy storage: A review. *Appl. Therm. Eng.* **2019**, *147*, 841−855.
(35) Drissi, S.; Ling, T.-C.; Mo, K. H. Thermal efficiency and durability performances of paraffinic phase change materials with enhanced thermal conductivity − A review. *Thermochim. Acta* **2019**, *673*, 198−210.
(36) Leong, K. Y.; Abdul Rahman, M. R.; Gurunathan, B. A. Nano-enhanced phase change materials: A review of thermo-physical properties, applications and challenges. *J. Energy Storage* **2019**, *21*, 18−31.
(37) Bick, A. D.; Tang, S. K. Y. Effect of volume fraction on droplet break-up in an emulsion flowing through a microfluidic constriction. *Appl. Phys. Lett.* **2019**, *115*, No. 093702.
(38) Khor, J. W.; Jean, N.; Luxenberg, E. S.; Ermon, S.; Tang, S. K. Y. Using machine learning to discover shape descriptors for predicting emulsion stability in a microfluidic channel. *Soft Matter* **2019**, *15*, 1361−1372.
(39) Coley, C. W.; Thomas, D. A.; Lummiss, J. A. M.; Jaworski, J. N.; Breen, C. P.; Schultz, V.; Hart, T.; Fishman, J. S.; Rogers, L.; Gao, H.; Hicklin, R. W.; Plehiers, P. P.; Byington, J.; Piotti, J. S.; Green, W. H.; Hart, A. J.; Jamison, T. F.; Jensen, K. F. A robotic platform for flow synthesis of organic compounds informed by AI planning. *Science* **2019**, *365*, No. eaax1566.
(40) McClements, D. J. Edible nanoemulsions: fabrication, properties, and functional performance. *Soft Matter* **2011**, *7*, 2297−2316.
(41) Zhuang, T.-T.; Pang, Y.; Liang, Z.-Q.; Wang, Z.; Li, Y.; Tan, C.-S.; Li, J.; Dinh, C. T.; De Luna, P.; Hsieh, P.-L.; et al. Copper nanocavities confine intermediates for efficient electrosynthesis of C3 alcohol fuels from carbon monoxide. *Nat. Catal.* **2018**, *1*, 946.
(42) Cao, V. D.; Salas-Bringas, C.; Schüller, R. B.; Szczotok, A. M.; Hiorth, M.; Carmona, M.; Rodriguez, J. F.; Kjøniksen, A.-L. Rheological and thermal properties of suspensions of microcapsules containing phase change materials. *Colloid Polym. Sci.* **2018**, *296*, 981−988.
(43) Qiu, Z.; Zhao, X.; Li, P.; Zhang, X.; Ali, S.; Tan, J. Theoretical investigation of the energy performance of a novel MPCM (Microencapsulated Phase Change Material) slurry based PV/T module. *Energy* **2015**, *87*, 686−698.
(44) Qiu, Z.; Ma, X.; Zhao, X.; Li, P.; Ali, S. Experimental investigation of the energy performance of a novel Micro-encapsulated Phase Change Material (MPCM) slurry based PV/T system. *Appl. Energy* **2016**, *165*, 260−271.
(45) Yang, Y.; Guo, J.; Cheng, Z.; Wu, W.; Zhang, J.; Zhang, J.; Yang, Z.; Zhang, D. New composite viscosity reducer with both asphaltene dispersion and emulsifying capability for heavy and ultraheavy crude oils. *Energy Fuels* **2017**, *31*, 1159−1173.
(46) Marto, J.; Ascenso, A.; Simoes, S.; Almeida, A. J.; Ribeiro, H. M. Pickering emulsions: challenges and opportunities in topical delivery. *Expert Opin. Drug Delivery* **2016**, *13*, 1093−1107.
(47) Kundu, P.; Kumar, V.; Mishra, I. M. Modeling the steady-shear rheological behavior of dilute to highly concentrated oil-in-water (o/w) emulsions: Effect of temperature, oil volume fraction and anionic surfactant concentration. *J. Pet. Sci. Eng.* **2015**, *129*, 189−204.
(48) Pal, R. Effect of droplet size on the rheology of emulsions. *AIChE J.* **1996**, *42*, 3181−3190.
(49) Mabit, J.; Fayolle, F.; Legrand, J. Shear rates investigation in a scraped surface heat exchanger. *Chem. Eng. Sci.* **2003**, *58*, 4667−4679.
(50) Miyagawa, Y.; Katsuki, K.; Matsuno, R.; Adachi, S. Effect of oil droplet size on activation energy for coalescence of oil droplets in an O/W emulsion. *Biosci. Biotechnol. Biochem.* **2015**, *79*, 1695−1697.
(51) Csuka, Z.; Olšiak, R. *The Profile of Shear Stress in the Liquid at Turbulent Flow*; AIP Conference Proceedings; AIP Publishing, 2016; p 020032.
(52) Liu, Z.; Muldrew, K.; Wan, R. G.; Elliott, J. A. Measurement of freezing point depression of water in glass capillaries and the associated ice front shape. *Phys. Rev. E* **2003**, *67*, No. 061602.
(53) Domalski, E. S.; Hearing, E. D. Heat capacities and entropies of organic compounds in the condensed phase. Volume III. *J. Phys. Chem. Ref. Data* **1996**, *25*, 1−525.
(54) Abramov, S.; Berndt, A.; Georgieva, K.; Ruppik, P.; Schuchmann, H. P. Investigation of the influence of mean droplet size and shear rate on crystallization behavior of hexadecane-in-water dispersions. *Colloids Surf., A* **2017**, *529*, 513−522.
(55) El Rhafiki, T.; Kousksou, T.; Jamil, A.; Jegadheeswaran, S.; Pohekar, S. D.; Zeraouli, Y. Crystallization of PCMs inside an emulsion: Supercooling phenomenon. *Sol. Energy Mater. Sol. Cells* **2011**, *95*, 2588−2597.
(56) McClements, D. J.; Dungan, S. R.; German, J. B.; Simoneau, C.; Kinsella, J. E. Droplet Size and Emulsifier Type Affect Crystallization and Melting of Hydrocarbon-in-Water Emulsions. *J. Food Sci.* **1993**, *58*, 1148−1151.
(57) Zhang, P.; Ma, Z.; Wang, R. An overview of phase change material slurries: MPCS and CHS. *Renewable Sustainable Energy Rev.* **2010**, *14*, 598−614.
(58) Avella, M.; Cosco, S.; Di Lorenzo, M.; Di Pace, E.; Errico, M. Influence of $CaCO_3$ nanoparticles shape on thermal and crystallization behavior of isotactic polypropylene based nanocomposites. *J. Therm. Anal. Calorim.* **2005**, *80*, 131−136.
(59) Puupponen, S.; Seppälä, A.; Vartia, O.; Saari, K.; Ala-Nissilä, T. Preparation of paraffin and fatty acid phase changing nanoemulsions for heat transfer. *Thermochim. Acta* **2015**, *601*, 33−38.
(60) Qiu, Z.; Qin, C.; Peng, L.; Zhao, X.; Zhang, T.; Li, Z.; Li, C.; Zheng, Y. Physical instability suppression of microencapsulated phase change material (MPCM) suspensions. *J. Therm. Sci. Technol.* **2018**, *13*, No. JTST0033.

https://dx.doi.org/10.1021/acs.energyfuels.0c01776
Energy Fuels XXXX, XXX, XXX−XXX